J Biol Inorg Chem (2007) 12:377–391
DOI 10.1007/s00775-006-0195-5

ORIGINAL PAPER

Metal ion binding properties of *Tricium aestivum* E_c-1 metallothionein: evidence supporting two separate metal thiolate clusters

Estevão A. Peroza · Eva Freisinger

Received: 10 August 2006 / Accepted: 15 November 2006 / Published online: 9 January 2007

Abstract Metallothioneins are ubiquitous low molecular mass, cysteine-rich proteins with an extraordinary high metal ion content. In contrast to the situation for the vertebrate forms, information regarding the properties of members of the plant metallothionein family is still scarce. We present the first spectroscopic investigation aiming to elucidate the metal ion binding properties and metal thiolate cluster formation of the *Tricium aestivum* (common wheat) early cysteine-labeled plant metallothionein (E_c-1). For this, the protein was overexpressed recombinantly in *Escherichia coli*. Recombinant E_c-1 is able to bind a total of six divalent d^{10} metal ions in a metal thiolate cluster arrangement. The pH stability of the zinc and cadmium clusters investigated is comparable to stabilities found for mammalian metallothioneins. Using cobalt(II) as a paramagnetic probe, we were able to show the onset of cluster formation taking place with the addition of a fourth metal ion equivalent to the apo protein. Limited proteolytic digestion experiments complemented with mass spectrometry and amino acid analysis provide clear evidence for the presence of two separate metal thiolate clusters. One cluster consists of four metal ions and is made up by a part of the protein containing 11 cysteine residues, comparable to the situation found in the mammalian counterparts. The second cluster features two metal ions coordinated by six cysteine residues. The occurrence of the latter cluster is unprecedented in the metallothionein superfamily so far.

Keywords Metallothionein · Metal thiolate cluster · Zinc · Cadmium · Proteolytic digestion

Abbreviations

CD	Circular dichroism
DTT	Dithiothreitol
E_c-1	Early cysteine-labeled protein
ESI-MS	Electrospray ionization mass spectrometry
F-AAS	Flame atomic absorption spectroscopy
HEPES	4-(2-Hydroxyethyl)piperazine-1-ethanesulfonic acid
LMCT	Ligand-to-metal charge transfer
MCD	Magnetic circular dichroism
MT	Metallothionein
PAGE	Polyacrylamide gel electrophoresis
SDS	Sodium dodecyl sulfate
Tris-HCl	Tris(hydroxymethyl)aminomethane hydrochloride

Introduction

The superfamily of metallothioneins (MTs) [1] comprises a wealth of small (M_r < 10 kDa) cysteine- and metal-rich, presumably nonenzymatic proteins found in nearly all living organisms. Their primary physiological function is still a subject of controversy. Given the metal ion binding capacity of MTs, it is generally

Electronic supplementary material The online version of this article (doi:10.1007/s00775-006-0195-5) contains supplementary material, which is available to authorized users.

This article is dedicated to Prof. Bernhard Lippert on the occasion of his 60th birthday.

E. A. Peroza · E. Freisinger (✉)
Department of Chemistry,
University of Zurich,
8057 Zurich, Switzerland
e-mail: freisinger@aci.unizh.ch

considered that these proteins play a specific role in the storage of essential metal ions, such as Zn^{II} and Cu^{I}, and their transfer to various metalloenzymes and transcription factors, which are required during tissue repair, cell proliferation, and regeneration [2–4]. MT gene expression can be induced by certain metal ions as well as by a variety of physiological and chemical stressors (see [5] for an overview). The inducibility of most mammalian MTs by elevated metal ion levels points to a participation in metal detoxification by sequestering excess amounts of both essential and nonessential heavy-metal ions, e.g., Cd^{II} or Hg^{II} [6]. Another proposed function of MTs, which recently gained more attention, includes direct scavenging of cell-damaging reactive oxygen species [e.g., hydroxyl (•OH) and superoxide ($\bullet O_2^-$) radicals] accompanied by disulfide bridge formation and consequently also metal ion release [7–10]. All MTs share a pronounced affinity for metal ions with d^{10} configuration. Metal ions are bound via terminal and bridging thiolato atoms of the cysteine residues, resulting in metal thiolate clusters of defined stoichiometries. For divalent d^{10} metal ions, only two cluster arrangements have been structurally characterized, an M_3Cys_9 form found in vertebrate and crustacean MTs [11, 12] and an M_4Cys_{11} form present in vertebrates as well and in echinodermata MTs [11, 13]. A similar four-metal ion cluster, but with participation of histidine residues, $M_4Cys_9His_2$, was reported in the prokaryote *Synechococcus* sp. PCC 7942 [14]. Metal thiolate clusters of monovalent d^{10} metal ions, either in a native Cu^{I} form or in an artificial Ag^{I} form, have only been reported in two fungi species so far with stoichiometries of $M_{7–8}Cys_{10}$ [15] and M_6Cys_7 [16].

Little is known about the structure and function of family 15 MTs [17], the plant MT isoforms. They are subdivided into essentially four subfamilies, p1, p2, p3, and pec, on the basis of the number of cysteine residues per protein and their distribution along the peptide chain. With few exceptions, a typical plant MT is composed of 60–85 amino acids. The major feature of members of the plant p1, p2, and p3 subfamilies is the clustering of cysteine residues in the amino-terminal (N-terminal) and the carboxy-terminal (C-terminal) parts of the protein, separated by a long cysteine-free linker region with a typical length between around 30 and 45 amino acids. The cysteine pattern of the N-terminal region is strictly conserved within a subfamily and is one of the major distinguishing features between subfamilies. In contrast, the distribution of cysteine residues within the C-terminal part is distinctively shared by all three subfamilies.

Triticum aestivum (common wheat) early cysteine-labeled protein (E_c-1) was the first plant MT discovered more than 25 years after the first MT from equine renal cortex had been identified [18, 19]. E_c-1 belongs to the pec subfamily and as such has the highest cysteine content of all plant MTs [18, 20, 21]:

MG**C**DDK**C**G**C**AVP**C**PGGTG**C**R**C**TSARSGAAAG
E**H**TT**C**G**C**GE**H**C**G**C**N**P**C**A**C**GREGTPSGRANRR
AN**C**S**C**GAA**C**N**C**AS**C**GSATA(PG).

Members of the pec subfamily further differ from all other plant MTs in that they contain a third cysteine-rich region and two considerably shorter linker regions. They are devoid of any aromatic amino acids, except for two highly conserved histidine residues at the central cysteine-rich region. The cysteine pattern of this central region is identical to that found in the C-terminal cysteine-rich part of plant MTs from the other subfamilies. Examples for other members of the pec subfamily are found in *Zea mays* (maize) [22], *Oryza sativa* (rice) [23], *Sesamum indicum* (sesame) [24], and *Arabidopsis thaliana* (mouse-ear cress) [25]. Expression of the E_c proteins is restricted to developing seeds, as well as to embryogenic microspores and pollen embryoids [26]. The highest level of wheat E_c-1 messenger RNA is reached in immature wheat embryos approximately 15 days after anthesis and declines rapidly after imbibition of the dried seed prior to germination. This abundance of E_c-1 in the early developmental stages is similar to the expression profile of rat liver MT, whose neonatal levels are 20 times higher compared with MT levels in adult rats [27]. Thus, an analogous role of E_c-1 in Zn^{II} homeostasis during embryogenesis is feasible [20]. While induction of the mammalian MT-1 and MT-2 genes is heavy-metal-dependent and mediated by *cis*-acting metal responsive elements located upstream of the genes [28], such elements are absent from E_c-1 genes. Accordingly, addition of metal ions such as Zn^{2+} has no influence on wheat E_c-1 expression levels [20], and hence a detoxifying function with respect to exogenous metal ions as predicted for mammalian MTs seems unlikely. Instead, the 5′-flanking region of the E_c-1 gene comprises a responsive element for the phytohormone abscisic acid. Accordingly, E_c-1 expression is positively regulated as well as induced by abscisic acid [20]. Among others, abscisic acid is a growth inhibitor and promotes senescence, leaf, flower, and fruit abscission, as well as bud and seed dormancy. Expression of E_c-1 under such conditions of slowed growth or even controlled senescence might point to a role in scavenging of essential

metal ions from metabolized proteins and storage for future onset of plant development.

Up to the present, knowledge concerning plant MTs is predominantly restricted to the identification of the corresponding genes and their messenger RNA transcription levels in different plant tissues at varying developmental stages. Considerably less information is available covering the translational products, rarely ever dealing with the purified proteins. Even if so, these proteins are largely still linked to some kind of purification-assisting tag, which might influence the protein properties to a nonnegligible level.

In this work, we describe for the first time the overexpression of *T. aestivum* E_c-1 in its recombinant form. The hitherto unknown spectroscopic behavior of the protein in combination with metal ions is presented and discussed. Further, results from proteolytic digestion experiments strongly support the presence of two separate metal thiolate clusters in E_c-1.

Materials and methods

Chemicals and solutions

T. album proteinase K was from Qbiogene (Lucerna Chem, Lucerne, Switzerland) and all other enzymes were from Promega (Catalys, Wallisellen, Switzerland), Roche (Rotkreuz, Switzerland), or New England Biolabs (Ipswich, MA, USA). Luria–Bertani broth (Miller) was purchased from Chemie Brunschwig (Basel, Switzerland), dithiothreitol (DTT) from Molekula (La Tour du Pin, France), tris(hydroxymethyl)aminomethane hydrochloride (Tris–HCl) from Calbiochem (VWR International, Lucerne, Switzerland), $^{113}CdCl_2$ from Cambridge Isotope Laboratories (Innerberg, Switzerland), and Chelex® 100 resin from Bio-Rad (Reinach, Switzerland). All others chemicals were ACS grade from Fluka (Buchs, Switzerland) or Acros Organics (Chemie Brunschwig, Basel, Switzerland). The deionized water used for the preparation of solutions was vacuum-degassed for approximately 30 min and nitrogen-saturated for at least 1 h. Where strictly anaerobic conditions were required, solutions were rendered oxygen-free by three freeze–thaw cycles under vacuum.

Construction of plasmid

The *T. aestivum* E_c-1 gene (Swiss-Prot accession number P30569 [23]) was optimized for *Escherichia coli* codon usage and constructed of commercially obtained oligonucleotides (approximately 50-nt length each; Microsynth, Balgach, Switzerland) by PCR. The synthetic gene was cloned into the vector pTYB2 from the IMPACT^{TM}-CN system (New England Biolabs) using the NdeI and XmaI restriction sites. This strategy adds two additional amino acids (proline, glycine) to the C-terminus of the protein. The accuracy of the insert and the integrity of the plasmid were confirmed by DNA sequencing.

Protein overexpression and purification

T. aestivum E_c-1 was overexpressed in the protease-deficient *E. coli* cell line BL21(DE3) in the form of a fusion protein with a vector-derived C-terminal intein tag (protein self-splicing element) and a chitin-binding domain according to procedures described in the IMPACT^{TM}-CN manual [29]. To facilitate formation of the E_c-1 holo forms, growth media were supplemented with $ZnCl_2$ or $CdCl_2$, respectively, to a final concentration of 100 μM. Cells were harvested by centrifugation 6 h after induction and stored at –80 °C for further use.

All further purification steps were carried out under a flow of nitrogen gas and using degassed and nitrogen-saturated solutions. In a typical purification procedure, cells from an 800 mL bacteria culture were resuspended in 20 mL buffer (20 mM Tris–HCl, pH 7.5, 200 mM NaCl, 3 mM ascorbic acid, and 1 mM $ZnCl_2$ or $CdCl_2$, respectively) and ruptured by sonification. After centrifugation, the supernatant was applied to a chitin column (New England Biolabs). Following extensive washing with increasing salt concentrations (up to 1 M NaCl), on-column self-cleavage of the intein tag was induced with 50 mM DTT [in 20 mM 4-(2-hydroxyethyl)piperazine-1-ethanesulfonic acid sodium salt (HEPES–NaOH), pH 7.5, 200 mM NaCl] overnight at 4 °C and additionally for 4 h at room temperature. Eluted crude E_c-1 was dialyzed against 1 mM HEPES-NaOH (pH 8.5) and lyophilized prior to a final purification step with size-exclusion chromatography using a HiLoad 16/60 Superdex 75 pg column (GE Healthcare, Otelfingen, Switzerland) and a buffer containing 10 mM Tris–HCl (pH 8.5) and 50 mM NaCl. E_c-1 was eluted in a single peak, was again dialyzed against 1 mM Tris–HCl (pH 8.5), and was used directly for all pH titrations and metal ion substitution reactions, or was lyophilized and stored at –20 °C. Average yields were 2 mg of purified protein per liter of cell culture medium. Protein purity was examined with 12% sodium dodecyl sulfate (SDS) polyacrylamide gel electrophoresis (PAGE) using the Tris–tricine buffer system as described [30]. Monobromobimane-modified E_c-1 was prepared according to the literature method, but without addition of

EDTA or a reducing agent during the modification procedure [31].

Protein and metal ion quantification

E_c-1 concentrations were determined by quantification of thiolate groups with 2,2′-dithiodipyridine at pH 4.0 assuming all cysteine residues to be present in the reduced state [32]. Stoichiometric formation of thiopyridinone was followed via its absorption maximum at 343 nm (absorption coefficient 7,600 M^{-1} cm^{-1}). E_c-1 concentrations were calculated based on 17 cysteine residues present in the protein. The protein concentrations obtained are within the error limits and are in good agreement with values determined by amino acid analysis, corroborating the completely reduced state of the protein. Metal ion concentrations were accessed with flame atomic absorption spectroscopy (F-AAS) using an AA240FS spectrometer (Varian, Zug, Switzerland) in 0.2 M HNO_3 without further digestion of the protein matrix. The metal-to-protein stoichiometries obtained in this way were confirmed in metal ion substitution reactions (see later).

ApoE$_c$-1 preparation

ApoE$_c$-1 was prepared freshly prior to each experiment. Typically, 1 mg of $Zn^{II}E_c$-1 or $Cd^{II}E_c$-1 was dissolved in 250 μL of a 60 mM DTT solution and incubated for 1 h on ice. All subsequent steps were carried out in a nitrogen-purged glove box. The solution was acidified to pH 1 with 1 M HCl and applied to two sequentially connected 5-mL HiTrap™ desalting columns (GE Healthcare) preequilibrated with 10 mM HCl. The metal-free apo protein was manually eluted with 10 mM HCl using a syringe (flow rate approximately 3 mL min^{-1}). For all apoE$_c$-1 preparations, Zn^{II} and Cd^{II} concentrations were below the detection limit (0.001 ppm, F-AAS).

Reconstitution of Zn_6E_c-1 from apoE$_c$-1 for ESI-MS

ApoE$_c$-1 was mixed with 7 equiv of Zn^{2+} and the pH was raised to 8.6 with 1 M Tris solution, pretreated with Chelex® 100. After incubation with Chelex® 100 for approximately 10 min, the protein was dialyzed against 0.5 mM Tris–HCl (pH 8.6), concentrated by lyophilization, dialyzed against 5 mM ammonium acetate buffer (pH 8.5), and analyzed by electrospray ionization mass spectrometry (ESI-MS) at neutral pH (see later).

Metal ion titration of $Zn_{5.7}E_c$-1 and apoE$_c$-1

$Zn_{5.7}E_c$-1 (11 μM in 10 mM Tris–HCl, pH 8.6, 10 mM NaCl) was titrated with increasing amounts (0–9 equiv) of $CdCl_2$. After each metal ion addition, the solution was incubated for 20 min at room temperature and subsequently a UV spectrum was recorded. Metal ion reconstitution reactions of the apo protein were performed on freshly prepared apoE$_c$-1 in 10 mM HCl solution (see before) inside a nitrogen-purged glove box using vacuum-degassed and nitrogen-saturated solutions (see before). ApoE$_c$-1 solutions were supplemented with 10 mM NaCl and increasing amounts of $CdCl_2$ (0–8 equiv) or $CoCl_2$ (0–7 equiv, no NaCl added), respectively. For each incremental metal ion addition, a separate fraction of the apoE$_c$-1 solution was used. Finally, pH values were adjusted to 7.5 (±0.2) with 100 mM Tris solution and UV–vis spectra were recorded. The final concentrations for titrations with $CdCl_2$ were 10 mM NaCl, 1.5 mM Tris, and 7 μM E_c-1 (final volume 135 μL) and for titrations with $CoCl_2$ they were 7.7 mM Tris and 34 μM E_c-1 (final volume 155 μL).

pH titration of $Zn_{5.7}E_c$-1 and Cd_6E_c-1

An 800-μL aliquot of $Zn_{5.7}E_c$-1 (11 μM) or Cd_6E_c-1 (14 μM; 1 mM Tris–HCl, pH 8.6, 10 mM NaCl) was titrated with increments (typically 0.5–1 μL) of diluted HCl solutions. After each acid addition, the pH and a UV spectrum of the protein solution were recorded. Handling of samples throughout each experiment was under a flow of nitrogen gas. Dilution effects due to HCl addition were negligible. Curve-fitting of experimental data was performed with Origin 7.0 (OriginLab Corporation, Northhampton, MA, USA) and equations were derived as described later and in more detail in [33].

^{113}Cd NMR

$^{113}Cd^{II}E_c$-1 was prepared in a similar manner to a previously reported procedure [34]. $Zn_{5.7}E_c$-1 in 1 mM Tris–HCl (pH 8.5) was incubated with 7 equiv of $^{113}CdCl_2$ for approximately 10 min. Subsequently, the sample was treated with Chelex® 100 resin (4 °C, 2 h, gentle shaking) to remove nonbound metal ions, giving a ^{113}Cd to E_c-1 ratio of 6.1:1. The sample was lyophilized, redissolved in 99.8% D_2O supplemented with 50 mM NaCl, and the pH was adjusted to 8.5 (pD 8.9) with HCl. The final concentration of $^{113}Cd_{6.1}E_c$-1 was 5 mM in 50 mM NaCl and approximately 200 mM Tris–HCl. ^{113}Cd NMR spectra were recorded under

proton decoupling with a Bruker 500-MHz spectrometer (^{113}Cd, 111 MHz), equipped with a broadband observe probe head, relative to 1 M $Cd(ClO_4)_2$ at 20 °C with a 250-μL sample in a 5-mm Shigemi tube.

Limited proteolytic digestion

Cd_6E_c-1 was incubated with *T. album* proteinase K in an enzyme-to-substrate ratio of 1:50 for 40 min in a buffer containing 50 mM Tris–HCl (pH 8.0) and 10 mM $CaCl_2$. Subsequently, the digestion mixture was separated by size-exclusion chromatography using a Superdex Peptide 10/300 GL column (GE Healthcare, Otelfingen, Switzerland) and a buffer containing 60 mM ammonium acetate (pH 7.0).

UV absorption, CD and MCD spectroscopy

UV absorption measurements were carried out with a Cary 500 scan spectrophotometer (Varian) using scan speeds of 600 nm min^{-1} in the range 200–800 nm for Co^{II} titration experiments and 200–500 nm for all other experiments. Circular dichroism (CD) spectra were recorded using a J-715 spectropolarimeter (JASCO, Japan) with the following parameters: scan speed 10 nm min^{-1}, spectral range 220–380 nm (four spectra accumulation). For magnetic CD (MCD), a JASCO J-715 spectropolarimeter was employed as well, but complemented with a magnet of 1.5 T (15 kG), using a scan speed of 20 nm min^{-1} in the range 225–350 nm (four spectra accumulation). All spectra were recorded at room temperature.

ESI-MS

Samples were diluted with 0.2% formic acid/50% acetonitrile (pH 2) or 5 mM ammonium acetate in 50% methanol (pH 7.0–7.5), and mass spectra were recorded with a quadrupole time-of-flight Ultima API spectrometer (Waters, UK). Deconvolution of spectra was performed with the MaxEnt1 software.

Results

E_c-1 expression, purity, and metal ion content

The protease-deficient *E. coli* cell line BL21(DE3) was used as an expression host. As a further precaution to reduce the unresolved probability of proteolytic cleavage of plant MTs in vivo [35, 36], E_c-1 was fused to a larger well-expressed, and folded, protein as provided in form of the self-spliceable intein tag within the IMPACT^{TM} system (New England Biolabs). A C-terminal intein tag was chosen to guarantee the integrity of the E_c-1 carboxy end and ensure binding of solely fully translated fusion constructs to the chitin affinity column. Protein splicing of the intein tag is induced by thiol compounds; in this case DTT was used. This has the beneficial side effect of creating a reducing environment, thereby reversing or inhibiting undesired disulfide bridge formation and preserving the full metal ion binding ability of the cysteine residues. After cleavage, an additional purification step using size-exclusion chromatography is applied, with E_c-1 being eluted from the column in a single sharp peak. SDS-PAGE followed by silver staining shows holoE_c-1 to be free of any other protein impurities, but also reveals an apparent molecular mass slightly above 17 kDa and not around approximately 8 kDa as expected (Fig. 1).

Such unusual migration behaviors have been described for proteins containing disulfide bridges, which preclude sufficient binding of SDS owing to their compact structure, leading to a lower negative charge and consequently to a higher apparent molecular mass in the gel experiment [37, 38]. Increased apparent masses were described infrequently for MTs in the past and have been associated with an oxidative formation of multimeric species [39]. This clearly does not apply for E_c-1 as mercaptoethanol was added as a reducing agent to the SDS-PAGE sample loading buffer. Alternatively, and more likely here, not disulfide bridges but actually the metal thiolate clusters preserve the compact structure of the protein and restrict SDS

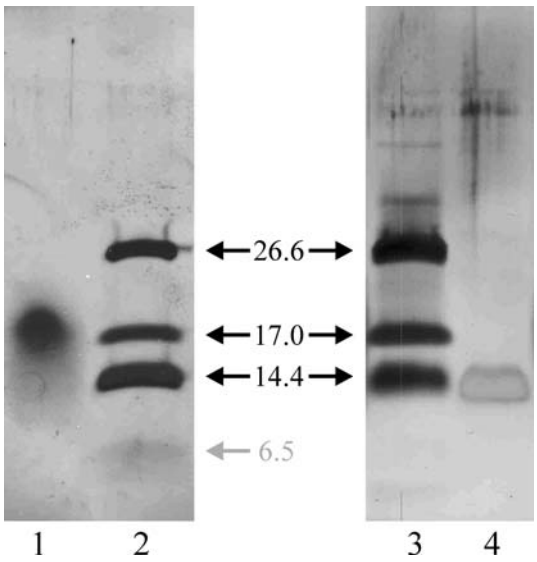

Fig. 1 Silver-stained SDS-PAGE (12%) of unmodified (*lane 1*) and monobromobimane-modified $Zn^{II}E_c$-1 (*lane 4*) relative to a peptide marker (*lanes 2, 3*). See also the text

loading to the surface of the protein. After disruption of the clusters by thiol modification with monobromobimane (see "Materials and methods"), the protein migrates slightly below the 14-kDa peptide marker line in SDS-PAGE (Fig. 1). A complete modification of all thiol groups would indeed increase the molecular weight of E_c-1 to approximately 11 kDa (8 kDa + 17 × 190.2 Da), thereby approximately fitting the experimental value. Considering further that the reactivity of monobromobimane is only directed towards thiol groups and not disulfide bridges, and that the modification was performed without addition of a reducing agent, E_c-1 must have already been present in its monomeric form before modification, or at least not as a disulfide-bridged multimeric species. Protein purity was also confirmed with ESI-MS of the apo (i.e., metal-free) forms at pH ~2 (Fig. 2a).

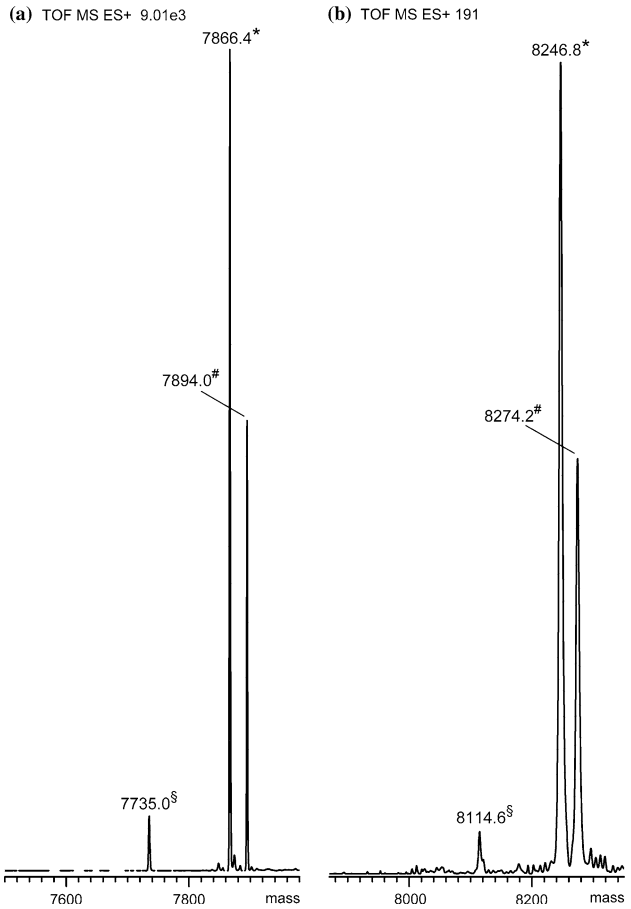

Fig. 2 ESI-MS spectra of E_c-1 in the metal-depleted apo form at pH 2 (**a**) or as the Zn_6 form at pH 7 (**b**). Each spectrum reveals three species: full-length, unmodified protein (*), full-length protein with formylation of the N-terminal methionine (#), and protein showing in vivo cleavage of the N-terminal methionine (§)

The mass spectrum shows a main peak corresponding to the full-length, unmodified protein at 7,866.4 Da (calculated 7,866.9 Da; average mass), a smaller peak caused by formylation of the N-terminal translation initiator methionine at 7,894.0 Da (calculated 7,894.9 Da), as well as a minor species which underwent cleavage of the N-terminal methionine at 7,735.0 Da (calculated 7735.7 Da). Both modifications are common features of proteins expressed in *E. coli* [40–43]. No further significant signals for protein impurities or for fragments indicating protein cleavage were detected.

Depending on the metal salt used for growth media supplementation ($ZnCl_2$ or $CdCl_2$), we obtain holoE_c-1 forms of the composition $Zn_{5.0–5.7}E_c$-1 or $Cd_{6.0}E_c$-1. The Zn^{II} content of the recombinant $Zn^{II}E_c$-1 forms directly isolated from the bacterial cells is thus only slightly higher than the value of five Zn^{2+} ions reported for E_c-1 isolated from wheat germ [21]. In contrast, reconstitution of apoE_c-1 with an excess of Zn^{2+} produces Zn_6E_c-1 in 100% yield as shown by ESI-MS (Fig. 2b), and this Zn_6E_c-1 species is even stable against treatment with Chelex® 100 (see "Materials and methods"). The maximum binding capacity of E_c-1 for Zn^{2+} is thus clearly 6. This is also confirmed for other divalent metal ions, taking into account recombinant Cd_6E_c-1 directly obtained from expression as well as the results obtained from various metal ion titration experiments (see later). The lower metal ion content of the recombinant or native $Zn^{II}E_c$-1 forms might indicate the presence of one weaker bound metal ion which might already be released at the pH values employed (see pH titration later) or upon interaction with weaker metal ion chelators such as the reducing agent DTT or the buffer Tris.

Metal thiolate cluster stability

Metal ion binding to and release from MTs can be conveniently followed by UV spectroscopy. The absorption spectra of the apo forms are characterized by a single absorption band around 190 nm, mainly due to transitions from the amide bonds, and complete transparency above 250 nm in the absence of the aromatic amino acids phenylalanine, tyrosine, and tryptophan, as is true, e.g., for mammalian MTs and also for members of the plant pec subfamily, including E_c-1. Upon metal ion binding, the characteristic ligand-to-metal charge transfer (LMCT) bands for metal thiolate clusters emerge, discernable by a more or less pronounced shoulder of the amide band (e.g. S → Zn around 230 nm, S → Cd around 250 nm; Fig. 3).

Both the Zn^{II} and the Cd^{II} forms of E_c-1 are stable against metal ion loss in an anaerobic environment at a

pH of around 8.5, even upon treatment with the metal ion chelator Chelex® 100. However, complete release of Zn^{2+} or Cd^{2+} ions is achieved by acidification below a pH of approximately 2.5. To determine apparent pK_a values of the cysteine residues in presence of the metal ion under investigation, $Zn_{5.7}E_c$-1 or $Cd_{6.0}E_c$-1, respectively, was treated with increasing amounts of hydrochloric acid and successive metal ion loss was monitored via the absorbance decrease of the respective LMCT bands. For data analysis, absorption at 230 nm ($Zn_{5.7}E_c$-1) or 250 nm ($Cd_{6.0}E_c$-1) is plotted against the pH value (Fig. 4).

The pH values of half dissociation of Zn^{2+} and Cd^{2+} from E_c-1 are 4.25 and 3.33, respectively, determined on the basis of half-maximum absorption. These values are significantly lower than those reported for the plant MT1–GST fusion protein from *Pisum sativum* MT1, 5.25 and 3.95, respectively [44], while they compare very well with values determined for equine MT: 4.50 [44] or 4.6 [19] for the removal of Zn^{2+} ions and 3.0 [19, 44, 45] for the removal of Cd^{2+} ions. The steep slope of the plots around the respective inflection points suggests that the majority of the metal ions is released at a given pH value and consequently the apparent pK_a values of most cysteine residues are obviously very similar. It seems therefore to be a valid simplification to neglect the concentrations of only partially protonated or deprotonated species and assume that only the completely protonated (E_cH_n) and deprotonated (E_c^{n-}) species contribute significantly to the UV absorption. As derived and explicated in [33], the total molar absorptivity A_{total} is then given according to

$$A_{total} = \frac{A_{E_c} + A_{E_cH_n} 10^{n(pK-pH)}}{1 + 10^{n(pK-pH)}}. \quad (1)$$

pK defines the single ''average'' apparent pK_a value for all cysteine residues in the presence of the metal ions under investigation and equals the pH value at half absorption, $1/2 \times (A_{E_c} + A_{E_cH_n})$. Equation 1 is actually just a different and more convenient setting of the Hill equation for this equilibrium, which could be equally used [33, 46]. n is identical to the Hill coefficient and can thus be seen as a measure of the degree of cooperativity governing the metal binding reaction. Fitting of n does not provide the exact number of protons released but can be alternatively used to estimate the minimal number of interacting binding sites. Curve-fitting of the pH titration data with Eq. 1 produces satisfactory results, especially for the titration of $Zn_{5.7}E_c$-1 (Fig. 4, Table 1).

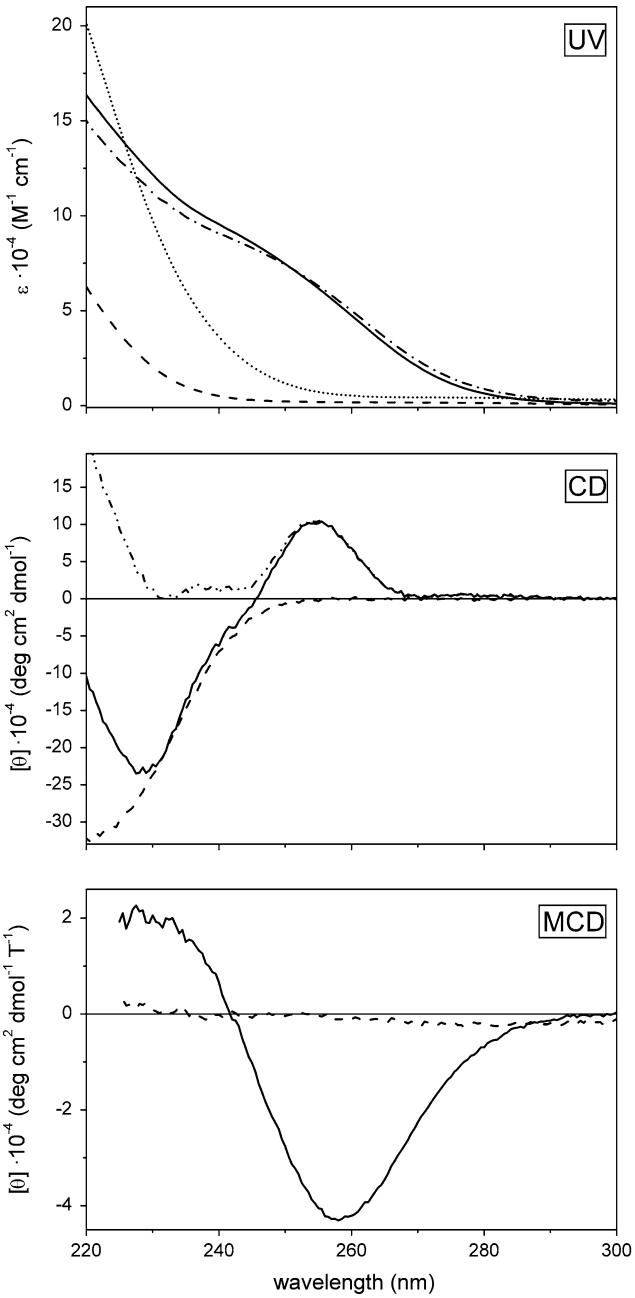

Fig. 3 UV, CD and MCD spectra of apoE_c-1 (*dashed lines*), $Zn_{5.7}E_c$-1 (*dotted line*, UV only), Cd_6E_c-1 (*solid lines*), and reconstituted Cd_6E_c-1 from apoE_c-1 (*dash-dotted line*, UV only). The *dash-dot-dotted line* in the CD spectrum was obtained by subtracting the apoE_c-1 spectrum from the Cd_6E_c-1 spectrum (named difference spectrum in the text)

Nevertheless, significant deviation from the experimental data is obvious at pH values above the inflection point in both plots; therefore, an additional model considering two different types of binding sites defined by two nonidentical apparent pK_a values was applied assuming the presence of two different types of protons, H_n and H_m [33]. The variables n and m again do

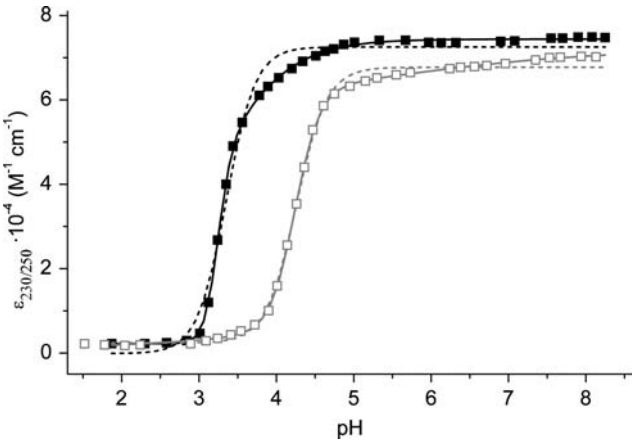

Fig. 4 Molar absorption versus pH for the pH titration of $Zn_{5.7}E_c$-1 (ε_{230nm}, *white squares*, translocated by –27,300 M^{-1} cm^{-1} to allow better comparability with Cd^{II} data) and $Cd_{6.0}E_c$-1 (ε_{250nm}, *black squares*), curve-fit with Eq. 1 (*dashed lines*), and curve-fit with Eqs. 2 and 3 (*solid lines*). See also Table 1

not result in the exact number of cysteine residues, but can be rather regarded as two different Hill-type coefficients. The corresponding two acid–base equilibria can be combined to yield either Eq. 2, when considering two interdependent apparent pK_a values, or Eq. 3, when assuming the contribution of two individual titration curves with a single pK_a value each to the total observed absorption:

$$A_{\text{total}} = \frac{A_{E_c} + A_{E_cH_m}10^{m(pK_2-pH)} + A_{E_cH_{n+m}}10^{npK_1+mpK_2-(n+m)pH}}{1+10^{m(pK_2-pH)}+10^{npK_1+mpK_2-(n+m)pH}}, \quad (2)$$

$$A_{\text{total}} = \frac{A_{E_cH_m} + A_{E_cH_{n+m}}10^{n(pK_1-pH)}}{1+10^{n(pK_1-pH)}} + \frac{A_{E_c} + A_{E_cH_m}10^{m(pK_2-pH)}}{1+10^{m(pK_2-pH)}}. \quad (3)$$

Both equations, Eqs. 2 and 3, fit both data plots equally well, yielding identical values for pK_1 within 1σ, respectively (see ''Discussion''). Values for n, pK_2, and consequently also for m show broader spreading. However, these values are not significantly different, having overlapping error limits (3σ). Although the first deprotonation steps at higher pH, characterized by pK_2, are obviously only poorly defined, considering these steps in the equations clearly improves the fitting for the pK_1 values.

Metal ion substitution and reconstitution

Substitution of Zn^{2+} ions by Cd^{2+} ions can be conveniently followed by UV spectroscopy as well. The pronounced shoulder resulting from the S → Cd transition around 250 nm is only marginally influenced by the S → Zn transition around 230 nm, making a correction for residual bound Zn^{2+} unnecessary in most cases. The absorption increases upon incremental addition of Cd^{2+}, reaching a plateau after 6 equiv (Fig. 5).

The same absorption increase up to 6 equiv can be observed upon reconstitution of apoE_c-1 with incremental amounts of Cd^{2+} (0–9 equiv, data not shown) or Co^{2+} (0–7 equiv, Fig. 6). After the addition of 3 equiv of Co^{2+} to the apo form, a gradual, mainly bathochromic shift of absorption bands (Fig. 6, insert) occurs until cluster formation is complete at 6 equiv and the protein is saturated with metal ions. In detail, the absorption spectrum of Co_6E_c-1 as well as the spectra of the substoichiometrically metal ion loaded forms are characterized by a minimum at 288–296 nm (Co_1E_c-1–Co_6E_c-1), followed by a maximum positioned at 310–319 nm ($\varepsilon = 20.6 \times 10^3$ M^{-1} cm^{-1} for Co_6E_c-1) with a pronounced shoulder around 380 nm ($\varepsilon = 15.0 \times 10^3$ M^{-1} cm^{-1}), all originating from S → Co charge-transfer transitions. The visible range of the spectra features the *d–d* transitions and is dominated by three broad bands, 614–628 nm ($\varepsilon = 1.6 \times 10^3$ M^{-1} cm^{-1}), 682–687 nm ($\varepsilon = 1.9 \times 10^3$ M^{-1} cm^{-1}), and roughly 747–739 nm ($\varepsilon = 1.3 \times 10^3$ M^{-1} cm^{-1}). The last band is again better described as a pronounced shoulder of the preceding absorption maximum, and in contrast to the other absorption bands reveals a slight hypsochromic effect with increasing metal ion content of the protein. The observed splitting into three absorption bands originates from spin–orbit coupling and has been

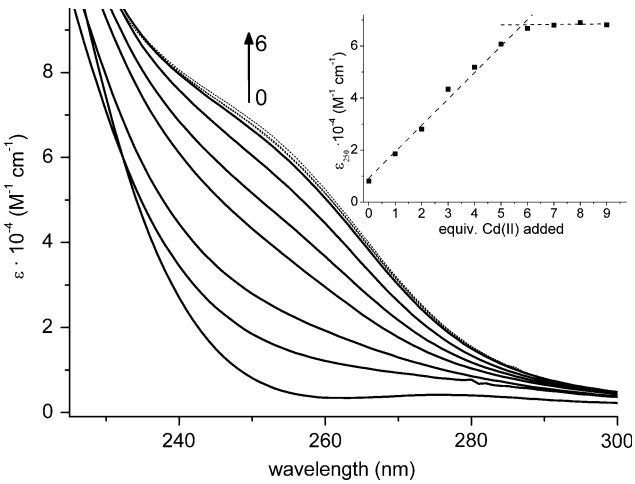

Fig. 5 UV spectra of the substitution of Zn^{2+} by Cd^{2+} in $Zn_{5.7}E_c$-1: 0–6 equiv (*solid lines*), 7–9 equiv (*dotted lines*). *Insert* Molar absorptivity at 250 nm against the number of equivalents of Cd^{2+} added. For a discussion, see the text

Table 1 Curve-fitting of pH titration data for $Zn_{5.7}E_c$-1 or $Cd_{6.0}E_c$-1 (see Fig. 4)

Equation 1	($Zn_{5.7}E_c$-1)	Equation 2	($Zn_{5.7}E_c$-1)	Equation 3[a]	($Zn_{5.7}E_c$-1)
A_{E_C}	95,189 ± 386	A_{E_C}	98,427 ± 1,640	A'_{E_C}	100,085 ± 923
		$A_{E_CH_m}$	90,583 ± 2,936	$A'_{E_CH_m}$	86,238 ± 479
$A_{E_CH_n}$	29,672 ± 505	$A_{E_CH_{n+m}}$	29,975 ± 210	$A'_{E_CH_{n+m}}$	29,046 ± 480
pK	4.26 ± 0.01	pK_1	4.24 ± 0.03	pK_1	4.240 ± 0.003
		pK_2	6.2 ± 0.5	pK_2	5.2 ± 0.2
n	2.2 ± 0.1	n	2.46 ± 0.06	n	2.73 ± 0.06
		m	0.5 ± 0.4	m	0.32 ± 0.05
Equation 1	(Cd_6E_c-1)	Equation 2	(Cd_6E_c-1)	Equation 3[a]	(Cd_6E_c-1)
A_{E_C}	72,530 ± 678	A_{E_C}	74,391 ± 150	A'_{E_C}	74,745 ± 1,948
		$A_{E_CH_m}$	21,898 ± 20,416	$A'_{E_CH_m}$	52,735 ± 1,906
$A_{E_CH_n}$	–117 ± 1,722	$A_{E_CH_{n+m}}$	2,213 ± 240	$A'_{E_CH_{n+m}}$	2,216 ± 1,687
pK	3.35 ± 0.02	pK_1	3.29 ± 0.02	pK_1	3.268 ± 0.005
		pK_2	3.3 ± 0.3	pK_2	3.9 ± 0.1
n	2.3 ± 0.2	N	4.5 ± 0.2	n	4.6 ± 0.3
		M	0.9 ± 0.1	m	1.3 ± 0.2

[a] The absorption values obtained from the original curve-fitting with Eq. 3 were shifted by $\{A_{E_CH_{n+m}}(\text{Eq. 2}) + |A_{E_CH_{n+m}}|(\text{Eq. 3})\}$ to result into A′ and allow direct comparison with values from Eq. 2

attributed to tetrahedrally coordinated high-spin Co^{II} tetrathiolate complexes [47, 48]. The intensity of the bands in the *d–d* region approximates about 10% of the absorptivity for the transitions in the LMCT region. The intensities of the bands in the visible range relative to each other change during the metal ion titration from 1.0:1.8:1.1 (614 nm:682 nm:747 nm) to 1.0:1.1:0.8 (628 nm:687 nm:739 nm). Additionally, while the spectra resulting from 1 to 3 equiv of Co^{2+} added to E_c-1 can be satisfactorily fitted with three Gaussian peaks, the fitting improves for higher metal ion contents if a minor additional peak located around 660 nm is considered, accounting for a slight shoulder of the band around 685 nm with lower wavelength (Fig. 6).

CD and MCD spectra

A detailed discussion concerning the chiroptical features of the Cd thiolate chromophore and their molecular origin has been presented in the literature [49]. The shape of the CD spectrum of Cd_6E_c-1 is remarkably similar to that of the CD spectrum of the Cd_4 α-domain of human growth inhibitory factor [50], with a maximum around 260 nm and a minimum roughly at 240 nm as well as an inflection point centered about the absorption maximum of the S → Cd LMCT band at 250 nm (Fig. 3, middle). Such features have been associated with the formation of a clustered structure [49, 50] and a comparison with CD spectra of

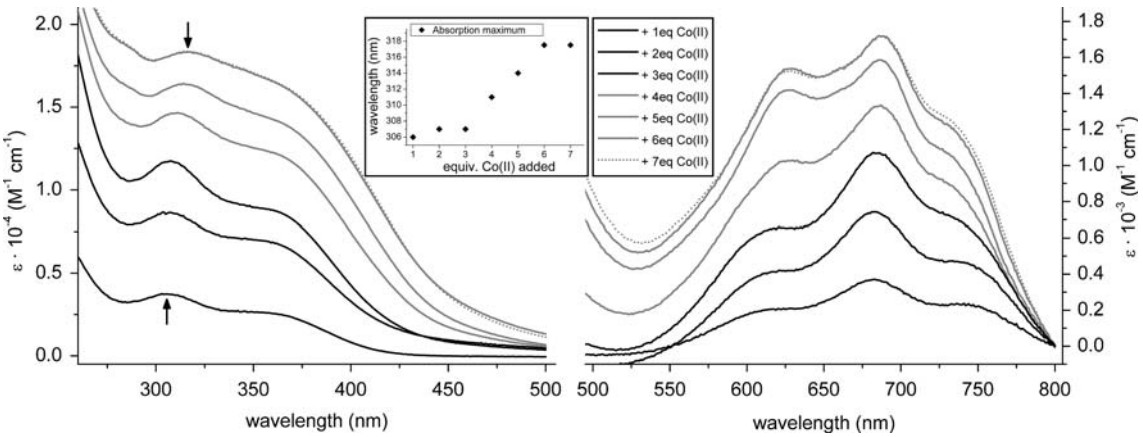

Fig. 6 Difference spectra of the reconstitution of apoE_c-1 (*dashed line*) with Co^{2+}: charge-transfer region (*left*), *d–d* transition region (*right*). Co^{2+} is bound to independent sites up to 3 equiv (*black lines*) and cluster formation occurs from 4 to 6 equiv (*gray lines*). Spectra obtained after addition of 6 or 7 equiv (*dotted gray lines*) of Co^{2+} are identical. The shift of absorption bands is most pronounced in the redshift of the local maxima around 310 nm (*insert*)

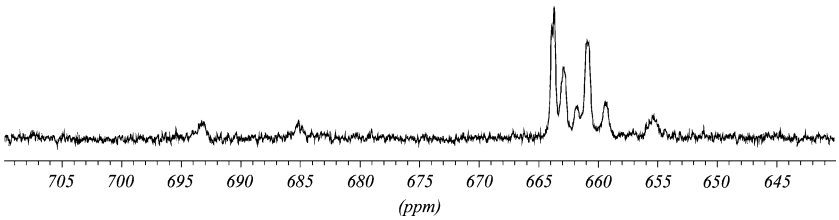

Fig. 7 1D ^{113}Cd NMR spectrum of $^{113}Cd_{6.1}E_c$-1, obtained by metal ion substitution of $Zn_{5.7}E_c$-1. Also the broad signals around 655, 685, and 693 ppm arise from the ^{113}Cd nucleus as shown by a ^{1}H–^{113}Cd heteronuclear single quantum coherence experiment

Cd^{II} MTs from other organisms and families is presented in Table 2.

The second positive CD band located around 225 nm in most MTs studied cannot be located unambiguously for Cd_6E_c-1 because of limitations in the spectral range of the measurement. Nevertheless, ellipticity clearly increases again after reaching the minimum at 229 nm. This second maximum has been associated with an additional higher-energy Cd thiolate transition and is clearly induced by the Cd thiolate cluster formation [47]. The locations of the extrema in the CD spectrum of Cd_6E_c-1 are all slightly shifted to lower wavelength compared with other full-length Cd-containing MTs (Table 2). In contrast to difference CD spectra of other Cd^{II} MTs, the difference CD spectrum of Cd_6E_c-1 does not show the typical biphasic behavior as the characteristic negative ellipticity band located around 240 nm and separating the two maxima is replaced by an area showing slight positive ellipticity (Fig. 3, middle). Differences from other MTs are less obvious when comparing the signals of the MCD spectra. Cd_6E_c-1 creates the typical features characteristic for MCD spectra of Cd^{II} MTs: a negative signal around 260 nm followed by a positive signal near 230 nm. The maximum in the present MCD spectrum is poorly resolved and is estimated to be centered around 230 nm.

^{113}Cd NMR

^{113}Cd NMR can be used to probe the coordination environment of Zn^{II} binding sites [51–53]. The chemical shift position of the ^{113}Cd resonance has been found at 600–700 ppm for a $^{113}CdCys_4$ cluster in eukaryotic MTs [51], at approximately 700–750 ppm for an isolated $^{113}CdCys_4$ cluster [54, 55], and in the range 630–660 ppm for a $^{113}CdCys_3His$ environment. The last region is thus not discernable from pure thiolate coordination [51]. Resonances for $^{113}CdCys_2His_2$ species are shifted further upfield (380–450 ppm) [51]. The 1D ^{113}Cd NMR (^{1}H-decoupled) spectrum of $^{113}Cd_{6.1}E_c$-1 reveals the presence of up to eight signals with chemical shifts between 655 and 695 ppm (Fig. 7), consequently being in the chemical shift range usually found for $^{113}CdCys_4$ or $^{113}CdCys_3His$ resonances in clustered structures.

However, 2D homonuclear ^{113}Cd-^{113}Cd correlation spectroscopy data of the same protein only reveal cross peaks between two of the signals (data not shown). A ^{1}H-^{113}Cd heteronuclear single quantum coherence spectrum shows cross peaks of protons to all seven (in this case) ^{113}Cd resonances of the 1D spectrum, thus verifying that also the broad signals around 655, 685, and 693 ppm in Fig. 7 are true ^{113}Cd resonances. No cross peaks were observed between $^{113}Cd^{2+}$ ions and protons of the histidine residues. Nevertheless, one needs to be aware that in all the spectra some of the resonances might not have been detected owing to chemical-exchange broadening [50], while additional peaks might be the result of chemical-exchange phenomena as well or a certain degree of protein oligomerization. Improvement of NMR signals by pH or temperature changes have been ineffective until now

Table 2 Location (nm) and sign of extrema in CD and MCD spectra of MTs from different organisms

Wheat Cd_6E_c-1	Snail Cd_6MT [64]	Human Cd_7GIF/ human Cd_4GIF [50]	Rabbit Cd_7MT [49]	Crab Cd_6MT [48]
CD				
(+) 255	(+) 256	(+) 259	(+) 259	(+) 261
(–) 229	(–) 242	(–) 235/(–) 230	(–) 240	(–) 245
(+) <220	(+) 220	(+) 225/(+) 220	(+) 224	(+) 235
MCD				
(–) 257		(–) 262		(–) 259
(+) ~230		(+) 237		(+) 228

GIF growth inhibitory factor

as have been trials with a ^{113}Cd form obtained by reconstitution of the apo form of the protein.

Proteolytic digestion

Proteolytic digestion of the peptide backbone of *T. aestivum* E_c-1 was performed with proteinase K, a subtilisin-related serine protease without pronounced cleavage specificity. Separation of the digestion mixture with gel filtration under nondenaturing conditions results into two peaks, both with longer retention times than the undigested protein, and a peak area ratio of roughly 2:1 (P1:P2, Fig. 8a). The concentrations of thiolate groups and metal ions in the central fractions of each peak were determined with the 2,2′-dithiodipyridine assay and F-AAS, respectively. The resulting thiolate-to-metal ion ratios were 2.74(6):1 for peak P1 and 2.98(7):1 for peak P2. The overall metal ion concentration in both peaks shows a ratio of roughly 1.6(1):1 (P1:P2). The ESI-MS spectrum of P1 (see the supplementary material) reveals the presence of two major signals, one at 1,904.9 Da matching the mass for residues 61–80 (calculated 1,906.2 Da) and the other at 2,566.1 Da corresponding to residues 31–56 (calculated 2,566.8 Da). Other minor signals can be assigned to fragments cleaved at slightly different positions, e.g., 2,637.7 Da corresponds to residues 30–56 (calculated 2,637.9 Da), 1,757.8 Da corresponds to residues 60–77 (calculated 1,761.0 Da), and finally 2,132.0 Da represents the intact C-terminus of the protein beginning with residue 61 (calculated 2,131.4 Da). The ESI-MS spectrum of P2 (see the supplementary material) is dominated by two signals at 2,448.1 and 2,317.0 Da representing the N-terminus of E_c-1 till residue 25 with methionine (calculated 2,448.9 Da) or without (calculated 2,317.7 Da). An amino acid analysis of P1 and P2 (Table 3) confirms the general assignment of the masses to the protein fragments. Deviations of the predicted amino acid content from the values found can to some extent be explained by the heterogeneity of the cleavage sites. Cysteine quantification was performed in a separate amino acid analysis experiment; however, substoichiometric values are found, which are due to the difficulty of the method for cysteine in general and particularly with cysteine-rich MTs.

Discussion

Metal thiolate cluster stability

Curve-fitting of the pH titration data with three different equations (Eqs. 1, 2, 3) yields mean apparent pK_a values (pK in Eq. 1 and pK_1 in Eqs. 2, 3) for the cysteine residues of 4.25 ± 0.01 ($Zn_{5.7}E_c$-1) and 3.30 ± 0.02 (Cd_6E_c-1; 3.28 ± 0.01 for curve-fitting with Eqs. 2, 3 only). As values obtained for the coefficient n are larger than unity (Table 1), addition of multiple protons, and release of multiple metal ions, seems to occur at pH values around the apparent pK_a, or, in virtue of the definition used in the Hill equation, metal-release from E_c-1 with decreasing pH is governed by a certain degree of cooperativity. The contribution of a preceding metal-release step taking place at a slightly higher pH is especially obvious in the pH titration of Cd_6E_c-1. This presumably two-step titration profile is far less pronounced than, for example, that observed for rabbit liver Cd_7MT-2a, and is more comparable to features found with human Cd_7MT-3 [56]. Accordingly, curve-fitting with Eqs. 2 and 3 gives relatively poorly defined values for pK_2, with mean values of 5.7 ± 0.5 ($Zn_{5.7}E_c$-1) and 3.6 ± 0.3 (Cd_6E_c-1), respectively, which render them actually indistinguishable from the respective pK_1 values within the 3σ significance level. However, if one assumes the presence of a two-step titration profile, though with relatively poorly resolved individual pK_a values, the decrease in absorbance between the $E_c^{(n+m)-}$ and a potential $E_cH_m^{n-}$ species could be taken as a rough measure for the number of metal ions released during this first cysteine protonation step. If one extrapolates the maximum absorbance of the fully deprotonated Zn^{II} form to Zn_6E_c-1 assuming linear behavior, the absorbance drop during the first protonation step will equal the release of 1.0 (fitting with Eq. 2) and 1.4 (Eq. 3) Zn^{2+} ions, respectively. For Cd_6E_c-1, curve-fitting with Eq. 3 would indicate the release of 1.8 Cd^{2+} ions (the σ value of $A_{E_cH_m}$ obtained with Eq. 2 is too high to provide any information). Such a two-step behavior could be an indication for the presence of two different metal thiolate clusters in E_c-1.

Metal ion substitution and reconstitution

Substitution of Zn^{2+} ions by Cd^{2+} ions in proteins, if (partially) bound to cysteine residues, usually results in the formation of isomorphous structures and is readily and stoichiometrically achieved owing to a generally higher binding affinity of Cd^{2+} ions for these sites. Implementation of Cd^{II}-substituted proteins has a number of advantages, including a generally higher stability against variations in pH and metal ion chelators, a more pronounced and thus easier to detect and quantify LMCT band, as well as the use of the ^{111}Cd or ^{113}Cd isotopes for NMR experiments. When following the substitution reaction of $Zn_{5.7}E_c$-1 with Cd^{2+} by UV

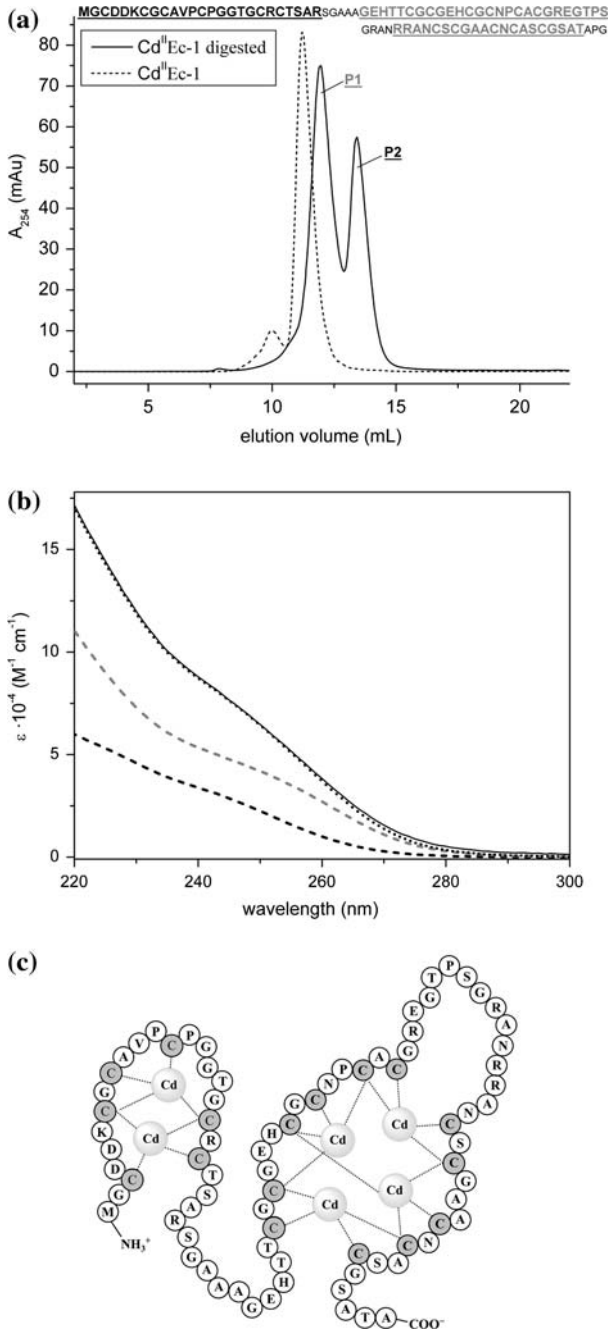

Fig. 8 **a** Gel filtration profile of undigested (*dotted line*) and proteinase K digested Cd_6E_c-1 with assignment of peaks to protein fragments (see Table 2). **b** UV spectra of peak P1 (calculation of ε based on 11 cysteines; *dashed gray line*), peak P2 (calculation of ε based on six cysteines; *dashed black line*), and undigested Cd_6E_c-1 (*solid black line*). Spectra were recorded in 50 mM NaCl and 10 mM Tris-HCI (pH 8.6). The summation of UV spectra from peaks P1 and P2 (*dotted black line*) superimposes very well with the spectrum of undigested E_c-1, supporting cluster integrity after digestion. **c** Metal thiolate cluster structure as evident from proteolytic digestion experiments. *Dotted lines* denote possible metal thiolate connectivities

Table 3 Amino acid analysis of products from proteolytic digestion of Cd_6E_c-1 (see Fig. 8a)

Amino acid	Peak 1		Peak 2	
	Calculated	Found	Calculated	Found
Glu (Gln)	**3**	**3.9**	**–**	**0.6**
His	**2**	**2.0**	**–**	**0.0**
Lys	**–**	**0.1**	**1**	**0.9**
Met	**–**	**0.3**	**1**	**0.5**
Val	**–**	**0.3**	**1**	**1.0**
Ala	7	5.5	2	2.3
Arg	3	2.2	2	1.7
Asp (Asn)	3	3.2	2	2.4
Cys	11	6.9	6	3.7
Gly	9	8.3	5	5.2
Pro	3	2.8	2	2.0
Ser	4	3.1	1	1.3
Thr	4	3.3	2	1.8
Iso	–	0.4	–	0.3
Leu	–	0.1	–	0.1
Phe	–	0.1	–	0.1
Tyr	–	0.0	–	0.0

Peak 1 contains the central and the C-terminal cysteine-rich regions of the protein, while peak 2 features the N-terminal part. Amino acids, which are theoretically only present in peak 1 or peak 2, but not in both, are marked in *bold*

spectroscopy, we observe maximum absorption at 250 nm after the addition of 6 equiv of Cd^{2+}. Additional Cd^{2+} shows no further effects. This finding is consistent with the metal-to-protein ratios found in the recombinant Zn^{II} or Cd^{II} forms of E_c-1 directly isolated from *E. coli*. The absorption increase does not seem to be strictly linear, especially upon addition of 5 and 6 equiv of Cd^{2+} (Fig. 5, insert). This behavior might be caused by an equilibrium reaction due to the competition of Cd^{2+} and Zn^{2+} for the same binding sites, consequently requiring the addition of superstoichiometric amounts of Cd^{2+}, e.g., 7 equiv, to achieve complete replacement of Zn^{2+} ions by Cd^{2+} ions.

To obtain MT derivatives of metal ions with lower affinities to thiolate groups than Zn^{2+} it is necessary to perform a reconstitution starting from the metal ion free apo form, usually prepared via acidification of the Zn^{II} or Cd^{II} forms to a pH below 2. To ensure that this rather harsh procedure preserves the general metal ion binding ability of E_c-1 after readjustment of the pH to neutral or slightly basic conditions, first reconstitutions with Zn^{2+} (see above) and Cd^{2+} were performed. Also with Cd^{2+}, a metal-saturated E_c-1 form is obtained after the addition of 6 equiv of Cd^{2+}. The spectra of Cd_6E_c-1 obtained after reconstitution or isolated directly from *E. coli* show the same absorption profile,

both in shape and in intensity (Fig. 3, top) confirming the integrity of E_c-1. The slightly higher absorption of the directly expressed Cd^{II} form around 230 nm (solid line) can be explained by an additional low Zn^{II} content, taken up from the culture medium during expression. The transition from an unclustered, i.e., solely binding of metal ions via terminal ligands, to a clustered structure with involvement of bridging ligands like thiolates can be unambiguously followed using Co^{II} owing to the sensitivity of its LMCT and *d–d* transition bands to changes in coordination geometry. The suitability of Co^{II} to serve as a paramagnetic probe for Zn^{II} in MTs and other Zn^{II}-containing proteins has already been shown [47, 57]. Particularly useful is that no cooperativity seems to be in effect when the metal ion binding sites in MTs are filled up with Co^{2+} ions. Thus, prior to the onset of cluster formation, all independent binding sites will be occupied; in other words, sites with terminal ligands only. As long as Co^{2+} binding occurs only to independent binding sites, solely an increase in absorption is observed. The onset of cluster formation is clearly marked by a shift in absorption bands as some terminal thiolate ligands become bridging. In the present titration of apoE_c-1 with Co^{2+}, this shift of absorption bands and thus the cluster formation starts with the addition of the fourth metal ion equivalent and is completed after binding of six Co^{2+} ions (Fig. 6, insert). The electronic spectra of $Co_{1-6}E_c$-1 are similar to spectra found and discussed for the Co^{2+}-substituted forms of other MTs. The mainly bathochromic effect observed in the course of the titration of E_c-1 corresponds to observations made for crab MT [48], while a progressive blueshift of the absorption band around 600 nm governs the spectra of rabbit liver Co_{1-7}MT-1 (shift from 610 to 590 nm) [47]. A marked difference of the Co_6E_c-1 spectrum compared with the spectra described for rabbit liver Co_7MT-1 and crab Co_6MT is found in the different intensities of the three absorption bands in the *d–d* region relative to each other: In Co_6E_c-1, the band at 628 nm is higher and the band at 739 nm lower than in the other two examples. It has been shown that replacement of one or two cysteine residues by histidine causes a relative increase in the highest-energy *d–d* transition around 650 nm for a $CoCys_3His$ [58] or $CoCys_2His(H_2O)$ [59] environment, an additional shift of this band to higher energy for $CoCys_2His_2$ coordination (635 nm) [60], as well as a complete disappearance of the lowest-energy *d–d* transition around 750 nm in all three cases. Thus, it might be reasonable to propose that the unusual relative intensities of the three *d–d* transitions observed for Co_6E_c-1 arise from the superposition of spectra from solely $CoCys_4$ sites with one or two $CoCys_3His$ sites or even a $CoCys_2His_2$ site. Alternatively, the observed intensity pattern could be also the result of a distinctively different cluster structure in wheat E_c-1 (see below). Further experiments will be needed to clarify this point.

With the Co^{2+} titration experiment three independent binding sites could be identified, which provides valuable information regarding the number and structure of metal thiolate clusters formed. The number of independent binding sites in a given cluster arrangement can be estimated by dividing the number of cysteine residues available by 4, thereby assuming tetrahedral coordination of metal ions and neglecting a possible participation of histidine residues. A hypothetical two metal ion cluster of the form M_2Cys_6 could then harbor one independent binding site, while the two clusters usually found in the well-studied MTs from families 1, 3, and 4, M_3Cys_9 and M_4Cys_{11}, provide sufficient ligands for the occupation of two independent binding sites each. One hypothetical ''super'' cluster, made up of all 17 cysteine residues, might accommodate four independent binding sites, if permitted by the rigidity of the peptide chain. On the basis of the stoichiometric considerations given above, E_c-1 can only feature either three separate M_2Cys_6 clusters or one M_4Cys_{11} and one M_2Cys_6 cluster (Fig. 8c), as both arrangements could accommodate a total of six metal ions and provide for three independent metal ion binding sites. In case of two separate clusters, metal ion binding could be achieved solely by making use of the 17 thiolate ligands, while in case of three clusters, an additional 18th ligand would be needed, which could be provided by, e.g., one of the highly conserved histidine residues as observed in bacterial MT forms [14]. Nevertheless, it should be noted that so far no cross peaks between $^{113}Cd^{2+}$ ions and protons of the histidine residues have been observed in ^{1}H-^{113}Cd heteronuclear single quantum coherence spectra (see before).

Proteolytic digestion

Proteolytic digestion was performed as an alternative way to address the so-far unresolved question concerning the number and size of metal thiolate clusters formed by E_c-1. It has been shown, that metal thiolate cluster formation protects the peptide backbone from cleavage under moderate digestion conditions [35, 61]. Even in the case of a certain degree of backbone cleavage between amino acids belonging to the same metal cluster, the integrity of the cluster under

nondenaturing conditions has been described [35]. In the case of *T. aestivum* Cd_6E_c-1, the digestion mixture is eluted from the gel filtration column in the form of two peaks, both with longer elution times and thus at a lower molecular mass than the undigested protein (Fig. 8a). This finding clearly excludes the formation of a single ''super'' cluster, which would be expected to be eluted in a single peak with approximately the same elution time as the undigested protein. It also rules out the presence of three separate M_2Cys_6 clusters, which should result in a single elution peak as well, given their similar hypothetical molecular masses, but with a considerably longer elution time than the undigested protein. Therefore, the proteolytic digestion experiment clearly implies the formation of two separate clusters with different molecular masses, in fact featuring roughly one third (P2) and two thirds (P1) of the full-length protein. Consistent with ESI-MS and amino acid analysis results, P2 represents the N-terminal cysteine-rich part of the protein, while P1 contains the central and C-terminal cysteine-rich regions. This assignment is further strengthened by the following two analytical results. First, only the ESI-MS spectrum of P2 shows signals differing by the mass of one methionine residue, typical for the N-terminus of the protein. Second, only the amino acid analysis of the P2 fractions reveals lysine, valine, and methionine, with half a methionine residue found being consistent with partial cleavage of the N-terminal methionine during expression, and strictly no histidine, while the results are the opposite for P1. The fact that ESI-MS reveals the presence of two different protein fragments in P1, which are coeluted from the gel filtration column, permits the conclusion that under the buffer conditions applied both fragments are connected by what is most likely a shared metal thiolate cluster. Using 8 M urea as a denaturing agent during gel filtration results in the same elution profile as before, thereby ruling out the possibility of any other noncovalently linked assembly of the two coeluted peptide fragments in peak P1. Summation of the two separate UV spectra obtained from the peak fractions of P1 and P2 yields a spectrum identical to that of undigested Cd_6E_c-1 (Fig. 8b). This finding further sustains the preservation of metal thiolate cluster integrity after digestion as well as the relative independence of the two clusters in the full-length protein. The thiolate-to-metal ratio of 2.98(7):1 found in peak P2 is consistent with an M_2Cys_6 arrangement (theoretical ratio 3:1). For P1 this ratio amounts to 2.74(6):1, reflecting the ratio expected for a cluster containing four metal ions and 11 cysteine residues (theoretical ratio 2.75:1; Fig. 8c). Final support for the presence of an M_2Cys_6 cluster in E_c-1 is provided by an ESI-MS spectrum of the P2 fraction at pH 7 (see the supplementary material), which shows a major signal at 2,668.0 Da fitting the mass of the N-terminus of the protein including methionine and two Cd^{2+} ions (calculated 2,667.7 Da). The smaller signal at 2,447.9 Da originates from the metal-depleted peptide (calculated 2,448.9 Da). Nevertheless, an ESI-MS spectrum showing the second cluster in an intact form could not be obtained yet, probably owing to a decreased stability of the half-digested cluster. Characterization of the separately expressed Cd_4 cluster is in progress at the moment. The occurrence of an M_2Cys_6 cluster is unprecedented in MTs so far, but is a well-known feature of transcriptional activator proteins, which have been studied in detail in yeast [62, 63]. Drawing any functional analogy to the members of the plant MT pec subfamily, however, seems far-fetched. For DNA recognition via two Zn_2Cys_6 clusters to be performed, these transcription factors need some kind of dimerization element to be able to relocate into their active homodimeric form. Whether and how the C-terminal Cd_4 cluster could inherit such a function is entirely speculative at this stage.

Using a combination of spectroscopic methods and biomolecular techniques, we were able to provide strong evidence for the presence of two different, relatively independent metal thiolate clusters in *T. aestivum* E_c-1, including their assignment to the N-terminal, M_2Cys_6, as well as the central and C-terminal part, M_4Cys_{11}, of the protein. Additionally, we could show a strong similarity between the spectroscopic features of E_c-1 and mammalian MTs, especially with respect to the pH stability of the metal thiolate clusters formed. Participation of the conserved histidine residues in the formation of the four metal ion cluster was not observed for the Cd^{II} form of the protein, but cannot be excluded entirely at this stage and thus has to be investigated further, especially for Zn_6E_c-1.

Acknowledgements We would like to thank T. Fox for the recording of NMR data, S. Chesnov (FGCZ, Zurich) for MS spectra and amino acid analyses, and M. Vašák (Department of Biochemistry, University of Zurich) for access to the MCD spectropolarimeter. Financial support from the Swiss National Science Foundation (project funding to E.F., 21-105269/1) and the University of Zurich (Forschungskredit 2004 to E.F.) is gratefully acknowledged.

References

1. Binz P-A, Kägi JHR (1999) In: Klaassen C (ed) Metallothionein IV. Birkhäuser, Basel, pp 7–13
2. Brouwer M, Winge DR, Gray WR (1989) J Inorg Biochem 35:289–303

3. Roesijadi G (1996) Comp Biochem Physiol C 113:117–123
4. Cherian MG, Kang YJ (2006) Exp Biol Med 231:138–144
5. Brady FO (1991) Methods Enzymol 205:559–567
6. Amiard J-C, Amiard-Triquet C, Barka S, Pellerin J, Rainbow PS (2006) Aquat Toxicol 76:160–202
7. Reinecke F, Levanets O, Olivier Y, Louw R, Semete B, Grobler A, Hidalgo J, Smeitink J, Olckers A, Van der Westhuizen FH (2006) Biochem J 395:405–415
8. Suzuki S, Tohma S, Futakawa N, Higashimoto M, Takiguchi M, Sato M (2005) J Health Sci 51:533–537
9. Feng W, Benz FW, Cai J, Pierce WM, Kang YJ (2006) J Biol Chem 281:681–687
10. Thornalley PJ, Vašák M (1985) BBA-Protein Struct M 827:36–44
11. Braun W, Vašák M, Robbins AH, Stout CD, Wagner G, Kägi JHR, Wüthrich K (1992) Proc Natl Acad Sci USA 89:10124–10128
12. Narula SS, Brouwer M, Hua Y, Armitage IM (1995) Biochemistry 34:620–631
13. Riek R, Precheur B, Wang Y, Mackay EA, Wider G, Guntert P, Liu A, Kägi JHR, Wüthrich K (1999) J Mol Biol 291:417–428
14. Blindauer CA, Harrison MD, Parkinson JA, Robinson AK, Cavet JS, Robinson NJ, Sadler PJ (2001) Proc Natl Acad Sci USA 98:9593–9598
15. Peterson CW, Narula SS, Armitage IM (1996) FEBS Lett 379:85–93
16. Cobine PA, McKay RT, Zangger K, Dameron CT, Armitage IM (2004) Eur J Biochem 271:4213–4221
17. Kojima Y, Binz P-A, Kägi JHR (1999) In: Klaassen C (ed) Metallothionein IV. Birkhäuser, Basel, pp 3–6
18. Hanley-Bowdoin L, Lane BG (1983) Eur J Biochem 135:9–15
19. Kägi JHR, Vallee BL (1960) J Biol Chem 235:3460–3465
20. Kawashima I, Kennedy TD, Chino M, Lane BG (1992) Eur J Biochem 209:971–976
21. Lane BG, Kajioka R, Kennedy TD (1987) Biochem Cell Biol 65:1001–1005
22. White CN, Rivin CJ (1995) Plant Physiol 108:831–832
23. http://au.expasy.org/sprot/
24. Chyan CL, Lee TT, Liu CP, Yang YC, Tzen JT, Chou WM (2005) Biosci Biotechnol Biochem 69:2319–2325
25. Cooke R, Raynal M, Laudie M, Grellet F, Delseny M, Morris PC, Guerrier D, Giraudat J, Quigley F, Clabault G, Li YF, Mache R, Krivitzky M, Gy IJ, Kreis M, Lecharny A, Parmentier Y, Marbach J, Fleck J, Clement B, Philipps G, Herve C, Bardet C, Tremousaygue D, Hofte H et al (1996) Plant J 9:101–124
26. Reynolds TL, Crawford RL (1996) Plant Mol Biol 32:823–829
27. Wong KL, Klaassen CD (1979) J Biol Chem 254:12399–12403
28. Koizumi S, Suzuki K, Ogra Y, Yamada H, Otsuka F (1999) Eur J Biochem 259:635–642
29. http://www.neb.com
30. Schagger H, Aquila H, Vonjagow G (1988) Anal Biochem 173:201–205
31. Meloni G, Knipp M, Vašák M (2005) J Biochem Biophys Methods 64:76–81
32. Pedersen AO, Jacobsen J (1980) Eur J Biochem 106:291–295
33. Freisinger E (2007) Inorg Chim Acta 360:369–380
34. Zangger K, Öz G, Otvos JD, Armitage IM (1999) Protein Sci 8:2630–2638
35. Kille P, Winge DR, Harwood JL, Kay J (1991) FEBS Lett 295:171–175
36. Robinson NJ, Wilson JR, Turner JS (1996) Plant Mol Biol 30:1169–1179
37. Valenzuela JG, Francischetti IMB, Pham VM, Garfield MK, Mather TN, Ribeiro JMC (2002) J Exp Biol 205:2843–2864
38. Pitt-Rivers R, Impiomba FSA (1968) Biochem J 109:825–830
39. Mounaji K, Erraiss NE, Wegnez M (2002) Z Naturforsch C 57:727–731
40. Liao YD, Jeng JC, Wang CF, Wang SC, Chang ST (2004) Protein Sci 13:1802–1810
41. Ozawa K, Headlam MJ, Schaeffer PM, Henderson BR, Dixon NE, Otting G (2004) Eur J Biochem 271:4084–4093
42. Ni X, Schachman HK (2001) Protein Sci 10:519–527
43. Giege R, Ebel JP, Clark BFC (1973) FEBS Lett 30:291–295
44. Tommey AM, Shi J, Lindsay WP, Urwin PE, Robinson NJ (1991) FEBS Lett 292:48–52
45. Kägi JHR, Vallee BL (1961) J Biol Chem 236:2435–2442
46. Hill AV (1910) J Physiol 40:4–7
47. Vašák M, Kägi JHR (1981) Proc Natl Acad Sci USA 78:6709–6713
48. Overnell J, Good M, Vašák M (1988) Eur J Biochem 172:171–177
49. Willner H, Vašák M, Kägi JHR (1987) Biochemistry 26:6287–6292
50. Vašák M, Hasler DW, Faller P (2000) J Inorg Biochem 79:7–10
51. Coleman JE (1993) Methods Enzymol 227:16–43
52. Goodfellow BJ, Lima MJ, Ascenso C, Kennedy M, Sikkink R, Rusnak F, Moura I, Moura JJG (1998) Inorg Chim Acta 273:279–287
53. Summers MF (1988) Coord Chem Rev 86:43–134
54. Bobsein BR, Myers RJ (1980) J Am Chem Soc 102:2454–2455
55. Pan T, Freedman LP, Coleman JE (1990) Biochemistry 29:9218–9225
56. Hasler DW, Jensen LT, Zerbe O, Winge DR, Vašák M (2000) Biochemistry 39:14567–14575
57. Vašák M (1980) J Am Chem Soc 102:3953–3955
58. Green LM, Berg JM (1989) Proc Natl Acad Sci USA 86:4047–4051
59. Sytkowski AJ, Vallee BL (1976) Proc Natl Acad Sci USA 73:344–348
60. Frankel AD, Berg JM, Pabo CO (1987) Proc Natl Acad Sci USA 84:4841–4845
61. Winge DR (1991) Methods Enzymol 205:438–447
62. Marmorstein R, Carey M, Ptashne M, Harrison SC (1992) Nature 356:408–414
63. Marmorstein R, Harrison S (1994) Genes Dev 8:2504–2512
64. Dallinger R, Wang YJ, Berger B, Mackay EA, Kägi JHR (2001) Eur J Biochem 268:4126–4133